Applied Catalysis A: General 475 (2014) 90–97

Contents lists available at ScienceDirect

Applied Catalysis A: General

journal homepage: www.elsevier.com/locate/apcata

Carbon nanotube/titanium nanotube composites loaded platinum nanoparticles as high performance photocatalysts

Mohamed M. Ibrahim[a], Saleh A. Ahmed[b], Khalid S. Khairou[b], Mohamed Mokhtar[c,*]

[a] Taif University, Faculty of Sciences, Chemistry Department, Al-Taif, Saudi Arabia
[b] Umm Al Qura University, Faculty of Applied Science, Chemistry Department, Abdia, Makkah, Saudi Arabia
[c] Benha University, Faculty of Applied Science, Chemistry Department, Benha, Egypt

ARTICLE INFO

Article history:
Received 12 October 2013
Received in revised form 8 January 2014
Accepted 13 January 2014
Available online 22 January 2014

Keywords:
Pt/TNT-MWCNT
Pt/graphene
Characterization
MB degradation
Mechanism

ABSTRACT

The multi-walled carbon nanotubes, titania nanotubes, and Pt metal (Pt/TNT-MWCT) hybrids; synthesized via hydrothermal-deposition methods, were tested toward photocatalytic degradation of methylene blue (MB) dye under visible light ($\lambda > 420$ nm) in comparison with the binary hybrid Pt/TNT and Pt/graphene photocatalysts. These catalysts were characterized using X-ray diffraction (XRD), UV–vis diffuse reflectance (DRUV–vis), Fourier transform infrared spectroscopy (FTIR), N_2 sorptiometry, photoluminescence (PL) spectroscopy and transmission electron microscopy (TEM) attached with energy dispersive X-ray spectroscopy (EDX). DRUV–vis analysis confirmed the enhancement in the absorption of Pt/TNT following MWCNT incorporation. TEM images showed the coverage of MWCNTs by brookite TNT that has been substantiated by EDX. The higher photo-activity of Pt/TNT-MWCNT (100% degradation in 140 min under visible irradiation) was attributable to the better contact between MWCNT and TNT; exhibited via formation of the Ti—O—C bond, which promoted the charge separation and electron transportation. Reduced charge recombination was evidenced for Pt containing samples and a further reduction was existed following MWCNTs incorporation; as investigated by PL measurements. The adsorption of MB by MWCNTs played major role in the removal efficiency. On the other hand, Pt/graphene presented appreciable activity, however, lower than Pt/TNT-MWCNT both in UV and vis light spectral regions due to decreasing the photocatalytic effect of the former than that of the latter. A mechanism for the MB oxidation was proposed based on the obtained results.

1. Introduction

TNT is one of the promising nanostructured oxides with tubular structure but has no absorption in the visible light region [1]. Researchers have fabricated a variety of geometric structures of TiO_2 nanoparticles including spherical nanoparticle, nanowire, nanorod and nanotubes [2–6]. TNTs are useful in dealing with waste-water due to the large surface to volume ratio. Most of synthesized TNTs are anatase in nature however, brookite is sometimes observed as a by-product when precipitation is carried out in an acidic medium [7]. Classically, brookite is obtained as large crystals by hydrothermal methods either in aqueous or in organic media [8] as well as when sodium cation content increases [9]. Brookite nanoparticles used to exhibit higher activity toward some reactions; such as methanol photooxidation and acetaldehyde degradation, than anatase nanoparticles [10]. This difference is explained by considering the crystallinity and the conduction band position, which is more negative than anatase. Generally, one main drawback of the TiO_2 nanostructure, when used in the practical application comes from their easy loss during water treatment. Attempts have been employed to improve the reuse efficiency of TiO_2, via the immobilization onto some supports such as carbon nanotube (CNT), glass, ceramic and activated carbon [11–14]. CNTs were chosen as support to increase remarkably the photoactivity of TiO_2 [15,16] through hindering electron–hole pair recombination. Accordingly, the aim of this work is to prepare a novel brookite TNT of nanospindle structure coating an oxidized MWCNT to study their effects as hybrid nanostructures toward photocatalytic degradation of the MB dye. Assembling metal particles either in the wall of TNT and/or CNTs or both will indeed enhance their photoelectricity and catalytic properties. Therefore, Pt loaded TNT and TNT-MWCNT was synthesized; and tested as well, and the obtained results are discussed in relation to the factors contributing to the enhanced photoactivity. For comparison purposes, Pt/graphene was synthesized to figure out the effect of graphene higher conductivity and surface area values [17] than CNT, on the photoactivity performance.

* Corresponding author. Tel.: +20 21025384411\\206073049.
E-mail address: mohmok2000@yahoo.com (M. Mokhtar).

0926-860X/$ – see front matter © 2014 Elsevier B.V. All rights reserved.
http://dx.doi.org/10.1016/j.apcata.2014.01.030

2. Experimental methods

2.1. Synthesis of titanium nanotube supported platinum

1.5 g of TiO_2 anatase (Aldrich) was refluxed at 423 K with 100 ml 10 M NaOH solution for 24 h. This milky suspension was then filtered and washed with aqueous HCl (0.1 M) and distilled water till pH 7. It was then dried at 373 K for 10 h and finally heated at 350 °C for 6 h. The produced TNT was dispersed in 50 ml H_2O together with 2 ml of 0.5 M/L acetone. An adequate amount of H_2PtCl_6 solution; to prepare 3 wt.% Pt, was added drop-wisely onto the above suspension during stirring for 1 h. Accordingly, hydrazine hydrate that acts as reducing agent was dropped into the above mixture. This mixture was then evaporated at 324 K for 4 h and finally heated at 623 K for 6 h.

2.2. Synthesis of Pt/MWCNT-TNT nanostructures

MWCNTs (average diameter 3–10 nm and length 5–20 μm) were first oxidized [11] via refluxing at 393 K using mixed acids (H_2SO_4:HNO_3 = 3:1) for 30 min. It was then diluted with water, filtered and washed till pH 7 followed by drying in an oven at 343 K for 12 h. The hybrid nanostructures were prepared by slowly dropping TiO_2 anatase (Aldrich) dissolved in 75 ml NaOH of 10 M concentration into the acid-treated MWCNTs dispersed in water with the aid of ultrasonication to give composite containing 30% CNTs/TNT. This dark suspension was loaded into Teflon-lined stainless steel autoclave and stored at 423 K for 60 h. The produced precipitate was separated by centrifugation followed by washing with ethanol-water mixture. The collected materials were left to dry at 393 K and heated at 623 K for 6 h. A desired amount of the MWCNTs/TNT composite was dispersed in water followed by ultrasonication at 318 K for 30 min. An adequate amount of H_2PtCl_6 solution; to prepare 3 wt.% Pt, was added onto the above suspension during stirring for 1 h. Accordingly, hydrazine hydrate was dropped into the above mixture followed by evaporation at 324 K for 4 h and heating at 623 K for 6 h.

2.3. Synthesis of graphene supported Pt

Graphitic oxide was prepared from purified natural graphite using modified methods [18,19]. Briefly, 2 g graphite was added to 46 ml of concentrated H_2SO_4 under continuous stirring in an ice bath. 1 g $NaNO_3$ and 6 g $KMnO_4$ were then added slowly and successively. The ice bath was removed and the suspension was allowed to cool to room temperature. 92 ml of water was then added to above mixture. After 15 min, the above mixture was diluted to 280 ml using warm water. Following this, 30% H_2O_2 was added till the solution turned bright yellow. The suspension was filtered and the filter cake was washed with warm water, repeatedly. The residue was diluted using water and the resulting suspension was centrifuged. The product was dried under vacuum and stored in vacuum desiccators, until further use. One pot modified polyol method [20] was adopted to disperse Pt nanoparticles onto reduced graphene oxide (RG-O), using H_2PtCl_6 as a Pt source and polyethylene glycol and hydrazine hydrate as reducing agents for Pt precursor and G-O, respectively. 3 wt.% Pt metal loading prepared by the modified polyol process i.e. Pt ions [H_2PtCl_6–$6H_2O$ (40% Pt based, Sigma–Aldrich)] dissolved in PEG solution (2 g/100 ml), was added drop wise to the graphite oxide dispersed in 20 mL H_2O and ultrasonicated for 30 min at 318 K solution. The solution was continuously stirred while adding hydrazine hydrate in a stepwise way and increasing the reaction temperature to 60 °C. The reduction product was separated by filtration and then washed with large amounts of water several times to remove residual ions. The product was finally dried in an oven at 100 °C for 12 h and calcined at 623 K for 6 h.

2.4. Catalyst characterization

2.4.1. X-ray diffraction

The X-ray powder diffraction patterns of various solids were carried out using a Philips 321/00 instrument. The patterns were run with Ni-filtered Cu Kα radiation (λ = 1.541 Å) at 36 kV and 16 mA with scanning speed of 2° in 2θ min^{-1}. The XRD phases present in the samples were identified with the help of ASTM powder data files.

2.4.2. N_2 adsorption

The surface properties namely BET surface area, total pore volume (V_p) and mean pore radius (r) were determined from N_2 adsorption isotherms measured at 77 K using conventional volumetric apparatus. The samples were out-gassed at 473 K for 3 h under a reduced pressure of 10^{-5} Torr before starting the measurement. The total pore volume was taken from the desorption branch of the isotherm at P/P^0 = 0.98, assuming complete pore saturation. The amount of chemisorbed H_2 was measured using the same apparatus. The sample was first reduced with H_2 at 673 K for1 h and then cooled to room temperature in flowing He. H_2 gas was introduced into the sample at 298 K until no more adsorption was observed. The Pt dispersion was calculated considering a dissociative adsorption of H_2 on a Pt surface atom leading to a stoichiometric ratio, Pt:H equal to 1.

2.4.3. UV–vis diffuse reflectance and photoluminescence spectroscopy techniques

UV–vis diffuse reflectance spectra of various samples in the 700–300 nm range were obtained using a Jasco V-570 (serial number, C 29635) spectrophotometer, which attached to a diffuse reflectance accessory unit. The photoluminescence (PL) excitation and emission spectra were measured on a FL/FS 900 time-resolved fluorescence spectrometer.

2.4.4. Transmission electron microscope (TEM)

TEM micrographs were measured using a Philips; model Tecani Feil2, at an accelerating voltage of 200 kV. The powder samples were put on carbon foil with a microgrid. TEM images were observed with minimum electron irradiation to prevent damage to the sample structure. The elemental compositions of the composite material were investigated by energy-dispersive X-ray attached to the TEM equipment. The average particle diameter (d) was calculated by the following formula: $d = \Sigma_{nidi}/\Sigma_{ni}$, where ni is the number of particle, di is the diameter in a certain range, and Σ_{ni} is more than 100 particles on TEM images of the sample. Computer-assisted counting of nanoparticle images and automated image analysis based software package including KONTRON KS 400 (Zeiss–Kontron) was used.

2.4.5. Fourier transform infrared spectra (FT-IR)

The infrared spectra of the samples were recorded in the range of 400–1000 cm^{-1}. The method includes mixing few milligram of a fine powder of the sample with KBr powder in an agate mortar. The mixture was then pressed by means of hydraulic press. The transmission was automatically registered against wavenumber (cm^{-1}) using a PerkinElmer instrument (Spectrum GX), made in USA.

2.5. Measurements of photocatalytic activity

Dark (adsorption) experiments were carried out for 60 min under continuous stirring for better adsorption equilibrium of the

MB (350 mL, 20 ppm) onto the surface of catalyst (0.15 g). A 300 W tungsten halogen lamp equipped with a UVA responsive to 320–400 nm, with no glass bulb or radiation filter and presented strong emission lines at 325, 343, 365, 366 and 391 nm, manufactured by Vilber Lourmat, France was used as an UV light source (the average light intensity was 60 mW cm^{-2}). Further, a 300 W high-pressure Hg lamp for which the strongest emission wavelength is 420 nm (the short wavelength components ($\lambda < 420$ nm) of the light were cut off using a glass optical filter) was used as a vis light source (the average light intensity was about 120 mW cm^{-2}). The lamp was cooled with flowing water in a quartz cylindrical jacket around the lamp, and the ambient temperature was maintained during the photocatalytic reaction. At given time intervals, analytical samples were taken from the mixture and immediately centrifuged, then filtered through a 0.22 mm Millipore filter to remove the photocatalyst. The concentration of the filtrate was analyzed by checking the absorbance at 665 nm with a UV–vis spectrophotometer (Varian Cary 100). The reproducibility was checked by repeating the measurements at least three times and was found to be within the acceptable limit (5%). More details about the apparatus and the adopted procedure can be found elsewhere [21]. The photocatalytic activity of the Pt/TNT-MWCNT composite was tested using phenol degradation; for comparison purposes, in aqueous solution under visible light irradiation using the same photoreactor and at similar concentration.

For detecting the active species produced in the photocatalytic reaction, hydroxyl radicals (•OH), superoxide radical ($•O_2^-$) and holes (h^+) were explored by adding 1.0 mM isopropanol (IPA-a quencher of •OH), p-benzoquinone (BQ-a quencher of $•O_2^-$), and triethanolamine (TEOA-a quencher of h^+), respectively. The method was similar to the former photocatalytic experiments.

3. Results and discussion

3.1. XRD and TEM investigation

Fig. 1 shows the XRD pattern of TNT demonstrating the crystallized phases for the sample following hydrothermal treatment at 423 K for 20 h and finally calcined at 623 K. It yields brookite (1 2 1) nanoparticles as a major phase (90%) together with rutile (1 1 0) impurities (10%) [22]. Following doping of TNT by Pt, a marked decrease in all brookite peaks together with the development of a small one at $2\theta = 39.6°$ due to Pt (1 1 1) phase was observed. Pt indeed affects the intensity of brookite (1 2 1) plane and on the other hand causes vanishing brookite peaks at $2\theta = 56.2°$, 67° and 75.8°.

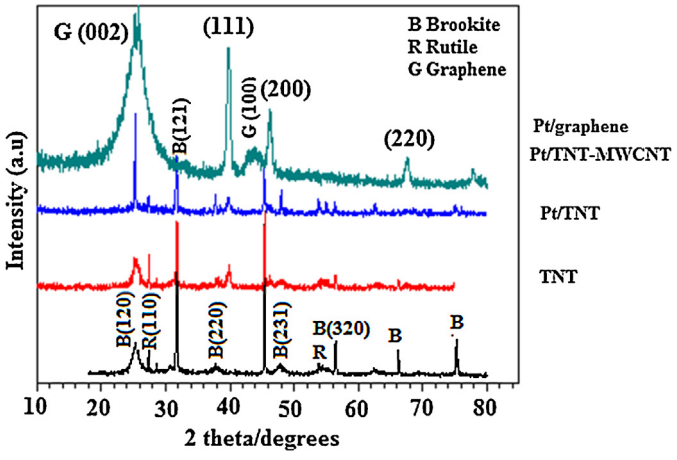

Fig. 1. XRD patterns of TNT, Pt/TNT, Pt/TNT-MWCNT and Pt/graphene photocatalysts.

Retaining TNT structure following MWCNT and Pt incorporations in the Pt/TNT-MWCNT pattern reflects the stability of the TNT structure, where the relative decrease in intensity of all TNT peaks concludes a decrease in its crystallites size. The change in the TNT peak shape at 25.5° following MWCNT(Pt) incorporation as well as its enhancement in intensity might be correlated to the superimposing of the brookite (1 2 0) peak over that of the CNT (0 0 2) one; assigned to graphitic basal plane reflection of CNTs. This proposes that a chemical interaction could have been occurred between OH groups of TNT and COOH groups exposed on the MWCNT surface. On the other hand, the diffraction pattern of Pt/graphene indicates characteristic peaks at 25.2° (0 0 2) and 44.0° (1 0 0) [23] correlated to graphene structure in addition to strong peaks at 40° (1 1 1), 46° (2 0 0) and 67° (2 2 0) consistent with the standard peaks of Pt nanoparticles of face centered cubic (fcc) structure [24]. Thus, Pt nanoparticles were highly dispersed in Pt/TNT and Pt/TNT-MWCNT materials unlike the case on graphene that exposed highly crystallized Pt nanoparticles.

The TEM image of TNT (Fig. 2a) shows that the particles are nanotubular in nature; and largely overlapping, having an inner diameter in the range 10–35 nm as well as length in the 80–120 nm range. As a magnified view, HRTEM in the inset figure showed open-ended tubes with multiple shells consisting of 3–6 layers, not always symmetric, with small dispersion in outer diameter (8–11 nm). In case of Pt/TNT, the nanotube structure changed into nanospindles (Fig. 2b) shape of length equal 150 nm and central width of 25 nm. For Pt/TNT-MWCNT, the TEM image (Fig. 2c) shows a clear change in the catalyst morphology acquiring nanotube titania shells enclosed MWCNT; as affirmed in the inset HRTEM micrograph, together with circular black Pt nanoparticles of average diameters equal 5–25 nm. It is also noted that the inner diameter of TNT became narrower following MWCNT incorporation; as seen in the inset figure. As a confirmation that TNT covers MWCNT, energy dispersive X-ray (EDX) elemental microanalysis (see supporting information) was carried out in selected areas in the inset Fig. 2c. It has been shown that C and O elements are richer in the MWCNT catalyst where the element carbon was absent in Pt/TNT pattern with the appreciable presence of Ti content. It can also be noticed that Pt was rich on the TNT surface where its absence on the surface of MWCNTs nullifies the diffusion of the Pt element @ MWCNT. Some impure elements are also existed probably from Pt precursor. Accordingly, it can be attested that the CNT/TNT composite was formed via using our adopted hydrothermal deposition method. The TEM image in Fig. 2d shows that graphene acquires nanoplates shape of average diameter ~20–50 nm. Obviously, Pt was sparsely decorated on graphene nanoplate surfaces and acquiring average sizes comprised of 20 ± 2 nm.

Fig. 3 depicts the IR spectra of the oxidized MWCNTs and the MWCNT/TNT composite. Bands at 1575, 1653 and 1713 cm^{-1} attributed to C=C, carbonyl and carboxyl, respectively were exhibited for MWCNT confirming its successful oxidization in addition to the presence an ester group localized as a strong band at 1175 cm^{-1}. The FTIR spectrum of MWCNT-TNT shows a peak at 700 cm^{-1} due to Ti—O—Ti vibration beside those exhibited for carbonyl and unsaturated carbon. The band intensity in the region of the asymmetric carboxylate stretching mode at 1400 cm^{-1} was significantly higher than that in MWCNT. This assumes that the carboxylate oxygen of CNT interacts with the titanium ion [25] provoking the Ti—O—C bond formation.

3.2. N_2 adsorption

Fig. 4a shows the adsorption–desorption isotherm of Pt doped graphene catalyst characterizing mesoporous structure. For TNT, the isotherm was of type IV (not shown) with a N_2 hysteresis-loop and a high surface area (240 m^2/g). The presence of Pt in TNT

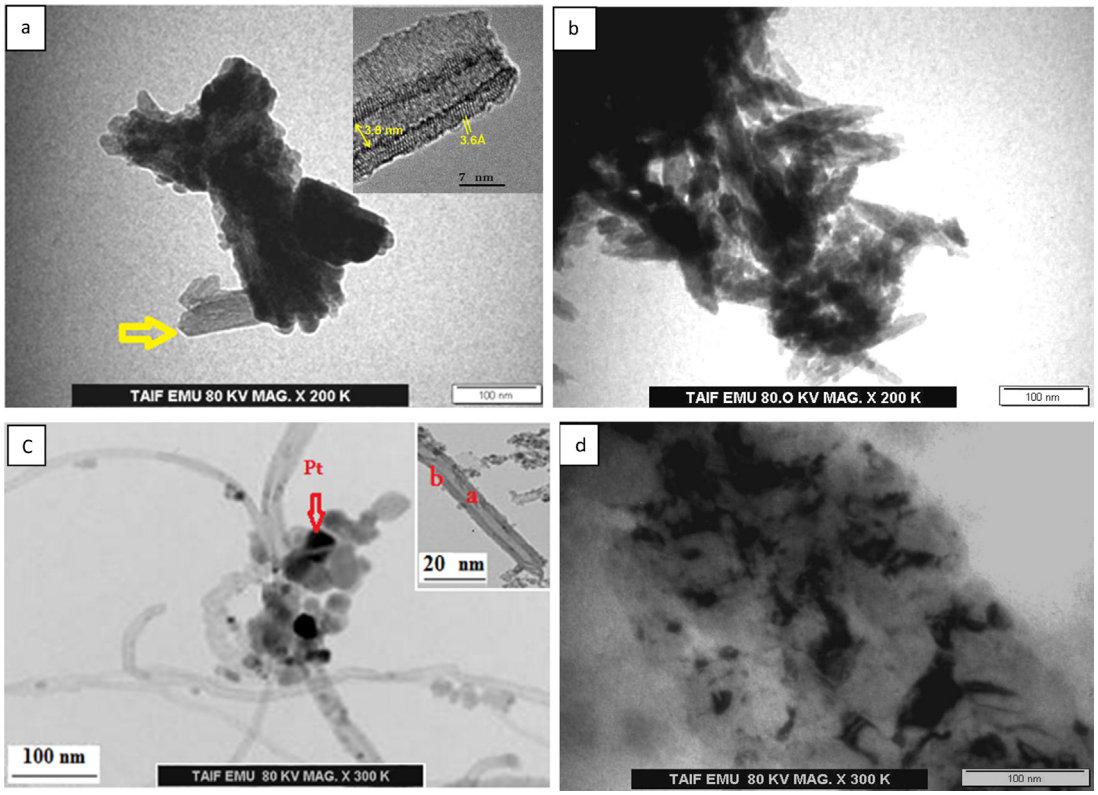

Fig. 2. (a) TEM image of TNT including HRTEM image (top-right inset showing the TNT tubular shape), (b) TEM Image of Pt/TNT nanospindle shape, (C) TEM image of Pt/TNT-MWCNT including HRTEM image (top-right inset showing the covering of MWCNT by TNT) and (d) TEM image of Pt/graphene nanoplate shape.

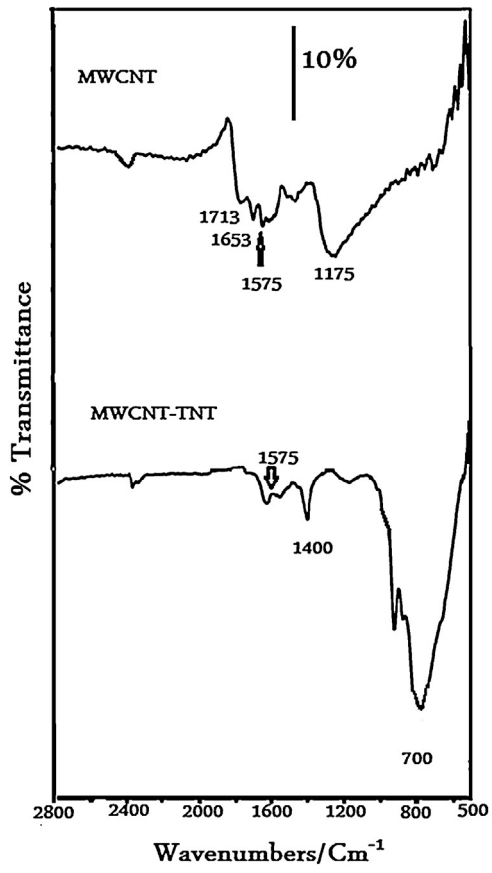

Fig. 3. FTIR spectra of oxidized MWCNTs and MWCNT/TNT composite.

led to a significant decrease in S_{BET} (192 m^2/g) comprised of 20% (Table 1). Incorporation of MWCNTs into Pt/TNT led to a further decrease in surface area of the composite (107.8 m^2/g). Accordingly, the pore volume of TNT, Pt/TNT and Pt/TNT-MWCNT showed a decrease comprised of 1.03, 0.9 and 0.051 cm^3/g, respectively (Table 1). The noticed incredible decrease in the pore volume of Pt/TNT-MWCNT into 0.051 cm^3/g might indicate the well incorporation of CNT into the TNT pores; as confirmed from TEM-EDX and IR investigations. It is well-known that the mesoporous structure is a more efficient photocatalyst structure for degrading organic pollutants in water. The specific surface area, pore volume and pore radius values of Pt/graphene were determined to be 78.5 m^2/g, 3.0 cm^3/g, and 15.3 nm, respectively. In the same time, the hysteresis loop of Pt/graphene closes at lower relative pressures $P/P^0 = 3.5$. This is indicative of the presence of large pores as ascertained from increasing the pore radius into 15.3 nm. Changing the desorption slope at $P/P^0 = 0.6$ is also indicative of the presence of two different types of pores. The adsorption–desorption isotherm of Pt/MWCNT-TNT carried out by N_2 adsorption at −197 °C is shown in Fig. 4b. The results confirm that the N_2 adsorption isotherm is belong to a mixed type, in the IUPAC classification, that composed of type II at high relative pressures (P/P^0) and type IV at intermediate relative pressures [26]. The non-limiting adsorption at high P/P^0 is characteristic of type H3. For comparison, the adsorption–desorption isotherm of Pt/TNT shown in Fig. 4c indicates type IV with type H3 hysteresis loop. The initial part of the type IV isotherm is attributed to monolayer–multilayer adsorption. Hysteresis appearing in the multilayer range of physisorption isotherms is usually associated with capillary condensation in mesopore structures. The Type H3 loop is observed with aggregates of plate-like particles giving rise to slit-shaped pores. Taking into account that titanate nanotubes are multiwalled rolls which are believed to be shaped via sheet folding or wrapping mechanism it seems to be reasonable that they exhibit the H3 loop.

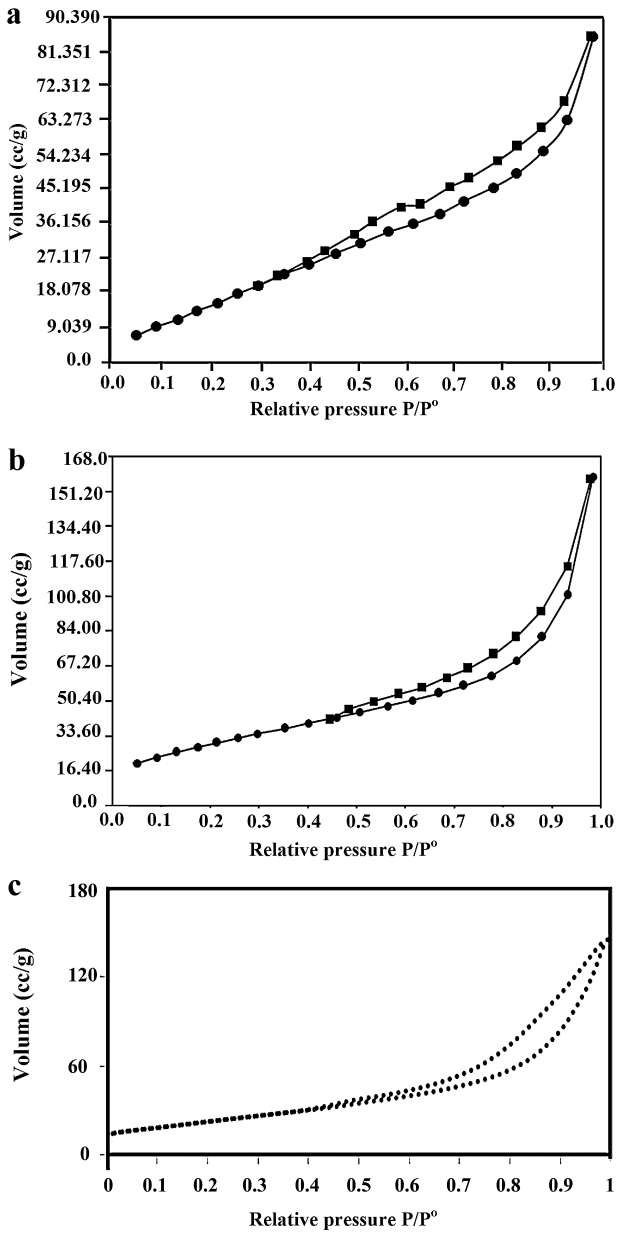

Fig. 4. adsorption–desorption isotherm of: 4 (a) Pt/graphene, 4 (b) Pt/TNT-MWCNT and 4 (c) Pt/TNT.

3.3. UV–visible diffuse reflectance spectroscopy

The light absorbing property of synthesized catalysts was measured by UV–vis diffuse reflectance spectroscopy (Fig. 5). Pure TNT shows characteristic absorption sharp edge at 325 nm beside an absorption maximum at 360 nm. The absorption threshold present in all spectra is attributed to an O_2^-:Ti^{4+} charge transfer of TiO_2 [27]. There is no indication of reduced titania sites; because no significant absorption is observed in the visible region, characteristic of d–d transitions. The diffuse reflectance spectra of Pt/TNT, Pt/TNT-MWCNT and Pt/graphene catalysts showed a red shift assigned to prevention of electron–hole recombination probably due to the formation of Pt-TNT, TNT-MWCNT and Pt-graphene bonds. An absorption around 450 nm assigned to surface plasmon caused by the metallic Pt is discerned in all Pt supported samples. Surface plasmon resonances in metallic nanoparticles are of interest for a variety of applications due to the large electromagnetic field enhancement that occurs near the metal surface and the dependence of the resonance wavelength on the nanoparticle size, shape and dielectric environment. Here we report an enhancement of optical absorption via the excitation of surface plasmon resonances in spherical Pt nanoparticles deposited on the different surfaces, arising from the collective oscillations of the free conduction-band electrons that are induced by the incident electromagnetic radiation. It seems that the incorporation of MWCNTs and graphene stimulate the absorption to be higher than TNT in the vis region, as they act as good electron acceptors capable of capturing electrons from light irradiation [28]. This exhibits that Pt/MWCNT-TNT and Pt/graphene composites will be more excellent photoactive than Pt/TNT. Interestingly, Pt/graphene exhibits the strongest absorption among those nanostructured carbon/TNT composites, proposing an intense electronic interaction between Pt and graphene. This discloses that CNT (graphene) possesses two kinds of crucial roles in the photocatalytic activity enhancement of TNT. One is to act as an electron container, helping to trap electrons emitted from TNT particles due to irradiation by UV/vis light,

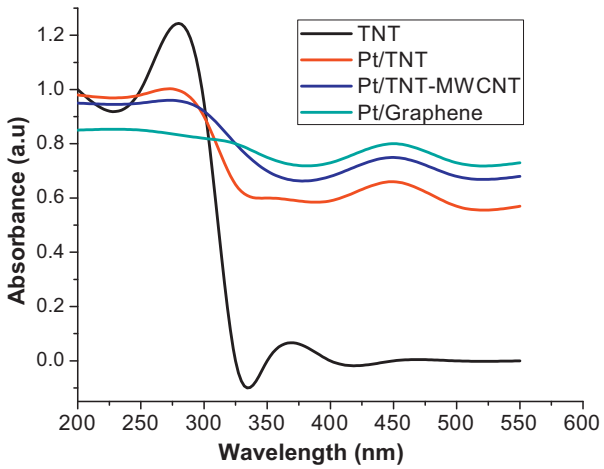

Fig. 5. UV–vis diffuse reflectance spectra of TNT, Pt/TNT, Pt/TNT-MWCNT and Pt/graphene photocatalysts.

Table 1
Surface texturing properties of the synthesized catalysts.

Sample name	[a]BET surface area (m^2/g)	[b]Pore volume V_p (cm^3/g)	[c]Average pore diameter (r nm)	[d]Fraction exposed (dispersion %)	[e]TOF min^{-1}
TNT	240	1.35	19.5	–	–
TNT-MWCNT	141	1.80	17.9	–	–
Pt/TNT	192	0.92	18.6	30 ± 1	0.025
Pt/TNT-MWCNT	107	0.05	17.5	37 ± 1	0.032
Pt/graphene	78.5	3.0	15.3	35 ± 1	0.029

[a] S_{BET}: BET surface area.
[b] V_p: Pore volume.
[c] r: BJH Adsorption average pore diameter.
[d] Pt dispersion measured by H_2 chemisorption.
[e] Number of moles of the product/number of active sites in moles x time.

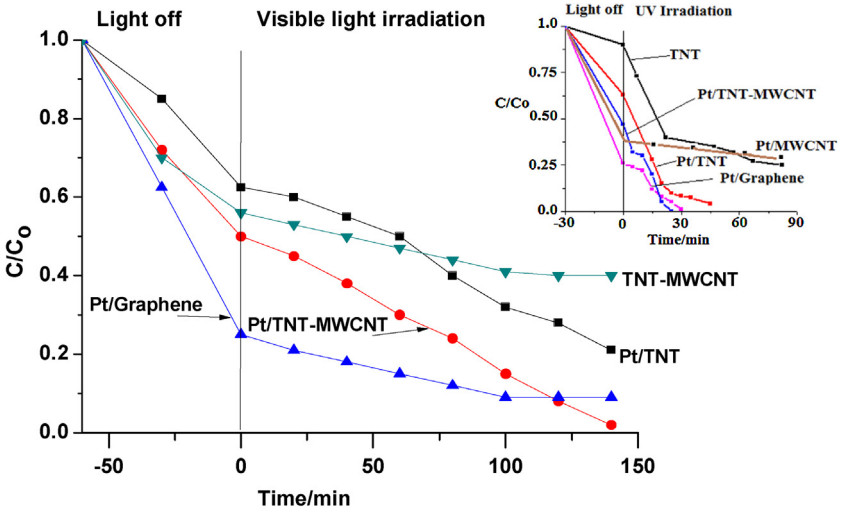

Fig. 6. Photocatalytic degradation of MB under the visible light and UV light (inset) irradiations over TNT, Pt/TNT, Pt/TNT-MWCNT and Pt/graphene photocatalysts. Reaction conditions: [MB] = 20 ppm, V = 0.35 L, [catalyst] = 1.5 g L^{-1}, UV lamp intensity = 60 mW cm^{-2} and vis lamp intensity = 120 mW cm^{-2}.

therefore hindering electron–hole pair recombination. The other is to function as a dispersing template or support to control the morphology of TNT particles in the CNT/TNT composite.

3.4. Photocatalytic evaluation

Photocatalytic performances of the different photocatalysts are evaluated by measuring their activities for MB degradation under UV and vis light irradiations (Fig. 6). The MB degradation in the absence of photocatalyst is exceptionally slow under both irradiations, because electron recombination between the injected electron and the excited dye*+ is fast in the photosensitization process. The high MB degradation in presence of TNT (75% in 90 min) under UV irradiations (Fig. 6-inset) is ascribed to the relatively simple combination between photo-ejected electron and adsorbed oxygen [27,28]. After the dispersion of Pt on TNT surface, the MB degradation is significantly increased (95% in 45 min). The reason for higher activity of the latter can be explained by considering the Pt nanoparticles to form locally Schottky junctions with a higher potential gradient at the Pt/TNT interface [29] based on exceeding the work function of the Pt than TNT [28]. On the other hand, the conduction band edge of TNT rich brookite has been found to be ~0.14 eV more negative than that of anatase [30]. This promptly suggests a facilitated interfacial electron transfer, and the energy barrier will suppress the electron back transfer. It is also obvious that Pt nanoparticles have strong influence on the photoactivity of MWCNT/TNT composite that showed remarkable adsorption reaching 55% for MB. Such light off experiments were continued till reaching the adsorption equilibrium (60 min). The favourable adsorption evoked by MWCNT is accomplished via π–π stacking between MB and aromatic regions of the MWCNT [31], exactly devoted for Pt/MWCNT that almost showed no activity under UV-light irradiation.

Although the surface area of Pt/TNT-MWCNT is lower than that of MWCNT-TNT (149 m^2/g), it exhibits higher photocatalytic activity (100% in less than 30 min under UV illumination) compared to the latter (85%-not shown). Considering the work function of MWCNT (4.95 eV) and TiO_2 (4.4 eV), excited MB can efficiently inject electrons into the TNT conduction band firstly, which can further move to MWCNT due to lowering the work function of TNT than MWCNT. This concludes that the degradation reaction by MWCNT/TNT can only be occurred for adsorbed MB on MWCNT surface, rather than on TNT surface. Owning to the work function of clean Pt is 6.10 eV [32], electron transfer from MWCNT to Pt is expected, and thus promoting the degradation of MB adsorbed on TNT/MWCNT surfaces. In the photo-degradation process by Pt/TNT-MWCNT composite, Pt nanoparticles act as a charge transfer channel [33] for enhancing the vis-light photoactivity of the composite (Fig. 6) to reach degradation comprised of 100% in 140 min exceeding the rest of catalysts. Surprisingly, Pt/graphene presented high activity (90% in 140 min), however, lower than Pt/MWCNT-TNT. The significant enhancement in the absorption of MB on Pt/graphene (75%); probably took place on the surface or between graphene sheets, was the priming effect on the removal efficiency than that of the photo effect exerted on Pt/MWCNT-TNT. On the latter, excellent electron transport (collect) properties [34,35] assist its forward transfer from photoexcited adsorbed dye molecules to Pt nanoparticles suppressing back electron transfer.

The electrons photogenerated in TNT following the irradiation move to the Pt metal through MWCNTs and thus the electrons on Pt metal participate in catalytic reactions i.e. MWCNT has the ability to trap electrons before channelling them to the conduction band of TNT. This proposes that the strong coupling between TNT and MWCNT; confirmed from TEM-EDX, IR and surface texturing results, affects the entire photodegradation process. Another reason is that MWCNT can absorb much oxygen on the inside or outside surface to act as an electron acceptor to form $^{\bullet}O_2^-$ that by its turn form $^{\bullet}OH$ through the presence of H^+. Thus, there may be more $^{\bullet}OH$ in the system throughout the MWCNT/TNT composite leading to faster degradation of MB. The inhibition effect of 2-propanol, which is known to be effective scavenging agent for hydroxyl radicals [36] was measured. As was shown (see Fig. in supporting information), the rate of MB degradation became slower at relatively low concentration of 2-propanol; while at high concentration of 2-propanol, great inhibition was observed indicating that the hydroxyl radicals are the major active species during the photo-catalytic oxidation reaction. >Further trapping experiments for detecting other active species was again conducted during the photocatalytic degradation of MB in the presence of Pt/TNT-MWCNT under visible light irradiation. As observed (see supporting information) the degradation efficiency of MB was not affected by the addition of 1 mM BQ (a quencher of $^{\bullet}O_2^-$), but apparently decreased with the addition 1 mM TEOA (a quencher of h^+). Therefore, the results show that $^{\bullet}OH$ and h^+ are the two main active species play key roles in the degradation of MB rather than $^{\bullet}O_2^-$. >A proposed mechanism for the enhanced photocatalysis of MWCNT/TNT doped Pt is shown

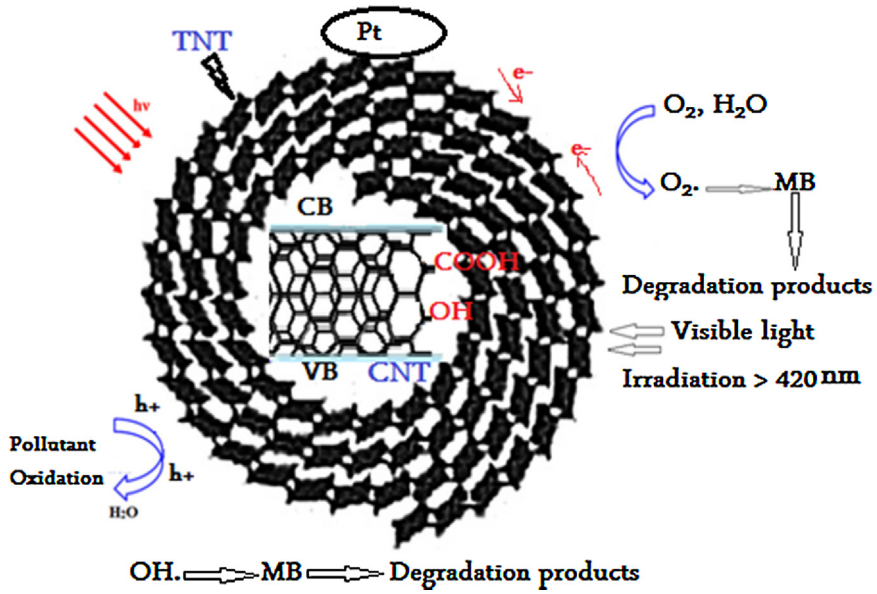

Fig. 7. The proposed photocatalytic mechanism of MWCNT/TNT/Pt catalyst under vis-light irradiation.

schematically in Fig. 7. Under vis light illumination, photo-excited electrons from the dispersed MWCNTs are injected into the conduction band of TNT affirmed through the combination of TNT-CNT i.e. the formation of the Ti—O—C bonds. The generated positively charged MWCNTs will in turn capture electrons from the valence band of Pt/TNT leaving holes behind on the TNT surface. Such holes can react with surface hydroxyl ions or water molecules to produce hydroxyl radicals (OH•). While electrons trapped by the Pt can react with adsorbed molecular oxygen yielding superoxide radicals ($O_2^{\bullet}$), which scavenge water molecules to form highly reactive OH• radicals. The OH• radicals are highly oxidizing agent and are capable of degrading MB to carbon dioxide and water. When TNT forms a heterojunction with MWCNT, a charge space ranging from several tens to hundreds of nanometres would be formed near the junction to equalise the Fermi levels [37]. This will result in reduced band-gap energy within the Pt/TNT/MWCNT heterojunction. In contrast, P25 gives (not shown) the lowest efficiency (4%) in the degradation of MB under the visible light irradiation, probably due to its large band gap. Pt/TNT catalyst indicates a conversion equal 95% under UV irradiation in 45 min where it presents 70% degradation efficiency when exposed to vis light for 140 min. In conformity, the turnover rates of the catalysts given in Table 1 indicate a decrease in the following order: Pt/TNT-MWCNT > Pt/graphene > Pt/TNT. There is a pronounced dependence of the turnover rate on the dispersion; i.e. the turnover number is increasing with higher dispersion and smaller particle sizes depicted from the TEM results. This finding indicates that the activity depends on the detailed surface structure of the nanoparticles and smaller particles are expected to expose a larger fraction of low-coordinated sites than larger particle. Accordingly, the high adsorption capability shown for Pt/graphene affected greatly the TOF rate compared with Pt/TNT-MWCNT.

In order to exclude the effect of photosensitization towards MB degradation, the photocatalytic conversion of phenol over the Pt/TNT-MWCNT catalyst under visible light irradiations was examined. It was shown that (see supporting information) the catalyst exhibited high adsorption capabilities (>50%) comparable to that noticed for the MB dye (~50%). Moreover, the activity of the mentioned catalyst revealed higher efficiency towards phenol degradation (120 min) compared with that of MB (140 min).

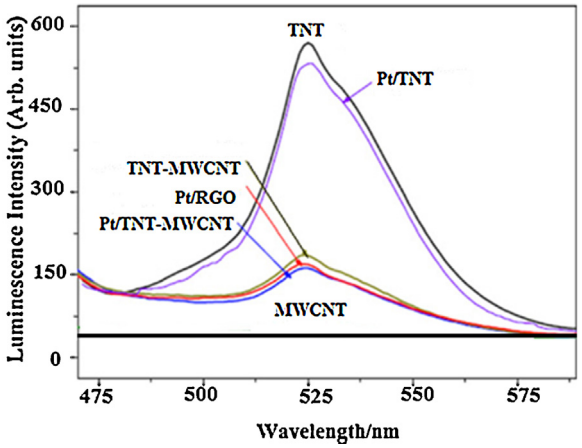

Fig. 8. PL spectra of MWCNT, Pt/TNT-MWCNT, Pt/graphene, TNT-MWCNT and TNT samples.

In order to study the effect of MWCNT on the recombination of e^-/h^+ produced by TNT, the PL spectra shown in Fig. 8 compares the e^-/h^+ recombination of Pt/TNT/MWCNT to those of Pt/graphene, Pt/TNT, TNT/MWCNT, TNT and MWCNT. Catalysts show broad PL emission bands, which were similar to those seen in an earlier study [38]. The emission band corresponding to the peak position of $\lambda = 520$ nm is for the TNT sample [39]. As expected, no PL signal is observed in the covered range for MWCNT. The Pt/TNT/MWCNT, Pt/graphene, Pt/TNT, TNT-MWCNT samples show diminished PL intensity indicating reduced charge recombination compared to TNT alone. This reduction increases for all Pt containing samples but more reduction was noticed in the samples containing MWCNT. This reflects that the structure of "dyade"-like is important for recombination reduction. On the base of our experimental data, it is proposed that the synergistic dyade structure of TNT/MWCNT provides access to optically active charge transfer transition. Under vis light irradiation, electrons (e^-) are excited from the valence band (VB) to the conduction band (CB) of TNT, creating a change vacancy, or a hole (h^+), in the CB. In the absence of MWCNT, most of these charges quickly recombine with no variation in chemistry. Typically, only few electrons (<1%) and holes are trapped and

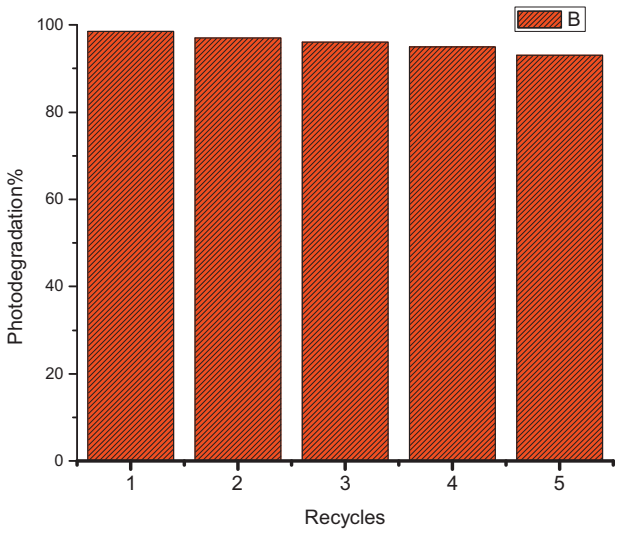

Fig. 9. Repeated cycles up to 5 times illustrating the degradation of MB dye after 170 min over the Pt/TNT/MWCNT photo-catalyst under vis light irradiation. Reaction conditions: [MB] = 20 ppm, V = 0.35 L, [catalyst] = 1.5 g L^{-1}, visible lamp intensity = 120 mW cm^{-2}.

participate in photocatalytic reactions, resulting in low reactivity. Accordingly, the synergistic effect caused by the chemical bond formation between d-orbital (CB) of TNT and Π orbital of MWCNT assists the transfer of excited electrons allowing charge separation and hindered recombination. The longer lived holes, on the other hand, are the ones responsible for the higher activity of the mentioned hybrid photocatalyst that has been substantiated with Pt nanoparticles.

To explore the advantage of the Pt/TNT/MWCNT catalyst and its applicability, reuse cycles of newly catalyst were tested for the degradation of MB dye (Fig. 9). Experiments were performed where the catalyst Pt/TNT/MWCNT was recovered and reused by keeping all other parameters constant. The results revealed that Pt/TNT/MWCNT shows a very good activity for five catalytic runs with a very small loss in the MB degradation. The conversion yield of Pt/TNT/MWCNT after 750 min was still as high as 93% even after the fifth run. It can be conclude that the Pt/TNT/MWCNT photocatalyst possesses reasonable stability and it may be reusable for at least 5 runs, showing a good potential for practical applications.

4. Conclusions

The results presented confirm the potential of the Pt/TNT/MWCNT composite for the degradation of MB dye as compared with those of TNT, Pt/TNT and Pt/graphene photocatalysts. The former exhibits excellent photocatalytic activity (100% degradation, vis irradiations) based on the adsorption effect promoted by MWCNT and electron trap achieved by Pt metal. The marked decrease in pore volume of Pt/TNT/MWCNT proposes that the interaction took place on the surface and also commits the inclusion of MWCNT in TNT as verified via the noticed increase in pore radius, TEM-EDX as well as IR investigations. This strong coupling between TNT and MWCNT gives advanced hybrid material of superior photocatalytic activity to other TNT and graphene based materials in the degradation of MB.

This work also elaborates a new method of synthesizing nanospindle brookite TNT that presented appreciable photoactivity under vis light upon loading with Pt nanoparticles.

Appendix A. Supplementary data

Supplementary data associated with this article can be found, in the online version, at http://dx.doi.org/10.1016/j.apcata.2014.01.030.

References

[1] S. Iijima, Nature 354 (1991) 56–58.
[2] Y. Feldman, E. Wasserman, D.J. Srolovitz, R. Tenne, Science 267 (1995) 222–225.
[3] H. Nakamura, Y. Matsui, J. Am. Chem. Soc. 117 (1995) 2651–2652.
[4] P. Hoyer, Langmuir 12 (1996) 1411–1413.
[5] T. Kasuga, M. Hiramatsu, A. Hoson, T. Sekino, K. Niihara, Adv. Mater. 11 (1999) 1307–1311.
[6] H. Masuda, K. Nishio, N. Baba, Jpn. J. Appl. Phys. 31 (1992) L1775–L1777.
[7] L.A. Bursill, J.L. Peng, L.N. Bourgeois, Philos. Mag. A 80 (2000) 105–117.
[8] F. Keller, M.S. Hunter, D.L. Robinson, J. Electrochem. Soc. 100 (1953) 411–419.
[9] N.G. Chopra, R.J. Luyken, K. Cherrey, V.H. Crespi, M.L. Cohen, S.G. Louie, A. Zettl, Science 269 (1995) 966–968.
[10] K. Ken-ichi, O. Yukiaki, T. Koji, T. Takaaki, M. Nobuhiro, O. Kiyoshi, ACS Appl. Mater. Interfaces 4 (9) (2012) 4846–4852.
[11] B. O'Regan, M. Grätzel, Nature 353 (1991) 737–739.
[12] G.H. Du, Q. Chen, R.C. Che, Z.Y. Yuan, L.M. Peng, Appl. Phys. Lett. 79 (2001) 3702–3704.
[13] Q.H. Zhang, L.A. Gao, J. Sun, S. Zheng, Chem. Lett. 31 (2002) 226–227.
[14] T.T. Lim, P.S. Yap, M. Srinivasan, A. Fane, Crit. Rev. Environ. Sci. Technol. 41 (2011) 1173–1230.
[15] B. Seger, P.V. Kamat, J. Phys. Chem. C 113 (2009) 7990–7995.
[16] R. Leary, A. Westwood, Carbon 49 (2011) 741–772.
[17] S. Yamanaka, T. Hamaguchi, H. Muta, K. Kurosaki, M. Uno, J. Alloys Comp. 373 (2004) 312–315.
[18] W.S. Hummers Jr., R.E. Offman, J. Am. Chem. Soc. 80 (1958) 1339.
[19] E.P. Lee, J. Chen, Y. Yin, T. Campbell, Y. Xia, Adv. Mater. 18 (2006) 3271–3274.
[20] T.K. Kasuga, A.H. Hiramatsu, A. Hoson, T. Sekino, K. Niihara, Langmuir 14 (1998) 3160–3163.
[21] M.M. Mohamed, M.S. Al Sharif, Appl. Catal. B 142–143 (2013) 432–441.
[22] V. Zwilling, E. Darque-Ceretti, A. Boutry-Forveille, D. David, M.Y. Perrin, M. Aucouturier, Surf. Interface Anal. 27 (1999) 629–637.
[23] W. Yang, X. Wang, F. Yang, C. Yang, X. Yang, Adv. Mater. 20 (2008) 2579–2587.
[24] S. Park, J. An, J.R. Potts, A. Velamakanni, S. Murali, R.S. Ruoff, Carbon 49 (2011) 3019–3023.
[25] L. Fuks, D. Filipiuk, M. Majdan, J. Mol. Struct. 792–793 (2006) 104–109.
[26] B. Chai, T. Peng, X. Zhang, J. Mao, K. Li, X. Zhang, Dalton Trans. 42 (2013) 3402–3409.
[27] M.A. Khan, H.T. Jung, O.B. Yang, J. Phys. Chem. B 110 (13) (2006) 6626–6630.
[28] M.M. Mohamed, K.S. Khairou, Microporous Mesoporous Mater. 142 (2011) 130–138.
[29] O.K. Varghese, D. Gong, M. Paulose, K.G. Ong, C.A. Grimes, Sens. Actuators B 93 (2003) 338–344.
[30] T.A. Kandiel, L. Robben, A. Alkaim, D. Bahnemann, Photochem. Photobiol. Sci. 12 (2013) 602–609.
[31] Y. Conga, X. Li, Y. Qina, Z. Donga, G. Yuana, Z. Cuia, X. Lai, Appl. Catal. B: Environ. 107 (2011) 128–134.
[32] R. Arsat, M. Breedon, M. Shafiei, P.G. Spizziri, S. Gilje, R.B. Kaner, K. Kalantarzadeh, W. Wlodarski, Chem. Phys. Lett. 467 (2009) 344–347.
[33] S. Takenaka, T. Arike, H. Matsune, M. Kishida, Appl. Catal. B: Environ. 125 (2012) 358–366.
[34] M. Gregory, C. Qiang, K. Alfred, W. Yue, Chem. Phys. Lett. 460 (2008) 517–520.
[35] Y. Si, E.T. Samulski, Chem. Mater. 20 (2008) 6792–6797.
[36] S. Kim, W. Choi, Environ. Sci. Technol. 36 (2002) 2019–2025;
Y.P. Huang, W.H. Ma, J. Li, M.M. Cheng, J.C. Zhao, J. Phys. Chem. B 107 (2003) 9409–9414.
[37] W. Sun, S. Zhou, B. You, L. Wu, Chem. Mater. 24 (19) (2012) 3800–3810.
[38] Y.S. Seo, C. Lee, K.H. Lee, K.B. Yoon, Angew. Chem. Int. Ed. 44 (2005) 910–913.
[39] G. Veréb, Z. Ambrus, Z.S. Pap, Á. Kmetykó, A. Dombi, V. Danciu, A. Cheesman, K. Mogyorósi, Appl. Catal. A: Gen. 417–418 (2012) 26–36.